



Stochastic-deterministic boundary element modelling of transcranial electric stimulation using a three layer head model

Anna Šušnjara^{a,*}, Ožbej Verhnjak^b, Dragan Poljak^a, Mario Cvetković^a, Jure Ravnik^b

^a University of Split, Faculty of Electrical Engineering, Mechanical Engineering and Naval Architecture, Split, Croatia

^b University of Maribor, Faculty of Mechanical Engineering, Maribor, Slovenia

ARTICLE INFO

Keywords:

Analysis of variance
Boundary element method
Stochastic collocation
Transcranial electric stimulation

ABSTRACT

This paper deals with the boundary element (BE) approach to modelling of transcranial electric stimulation as an alternative to the widely used finite element method (FEM). The advantages of the BE approach are listed in the paper and demonstrated on a computational example. The formulation is based on the quasi-static approximation of currents and voltages induced in living tissues while the head is represented by a three layered model consisting of skin, skull and brain tissues. Another contribution is the fact that the uncertainty present in the tissue conductivity values is taken into account by modelling them as uniformly distributed random variables. The stochastic collocation method (SCM) is applied for propagation of the uncertainty to the output electric scalar potential. Accordingly, stochastic moments are computed and sensitivity analysis is carried out using the ANalysis Of Variance approach (ANOVA). The results given in the paper show the efficiency of the BE-SCM combination. Inspecting the results obtained from the proposed BE-SCM approach it is clear that the confidence intervals are appreciably larger in the interior tissues. The impact of the skull's conductivity is shown to be negligible for most of the observation points while the skin and brain conductivities have a significant impact on the output value.

1. Introduction

The idea of brain stimulation by using the electric current is not new as it basically dates to the times of discovery of the electricity itself. Traditionally, the treatment of certain psychiatric disorders was conducted by using the strong electrical currents. However, some serious side effects have been reported, in particular the memory loss [1]. On the other hand, there has been an intensive research of the usage of the low-intensity currents going on, especially in recent decades. The principal mechanism of the action of the low-intensity transcranial electric stimulation (TES) is a subthreshold modulation of neuronal membrane potentials, which alters the cortical excitability and the activity dependant on the current flow direction through the target neurons [2,3]. An important difference compared to other non-invasive brain stimulation techniques such as transcranial magnetic stimulation (TMS) is that the activity in the resting neuronal networks is not induced, but rather the spontaneous neuronal activity is modulated. Consequently, the effects depend upon the previous physiological state of the target neural structures [2].

The low-intensity TES comprises techniques such as transcranial direct current stimulation (tDCS), transcranial alternating current stimulation (tACS), transcranial random noise stimulation (tRNS) and tran-

scranial pulsed current stimulation (tPCS) [1]. All four techniques are applied according to pre-established protocols and the procedures are reported to be well tolerated [1]. Many pieces of evidence indicate that the low-intensity TES plays an important role in the treatment of various neurological and psychiatric disorders such as depression, anxiety and Parkinson's disease [4,5]. However, despite the fact that the clinical experience and empirical research have resulted in the improvement of brain stimulation techniques, the underlying phenomena and the mechanisms of treatment are still not entirely understood [3]. Ongoing research activities in the field of computational modelling of TES aim to alleviate this problem with the main focus on the simulation of current distribution in the human head [6,7]. Computational modelling is a tool of a paramount importance for the design of TES electrode positions as different positions stimulate different parts of the cortex [8]. Moreover, due to differences in size and shape of each individual's head, a patient specific modelling may improve the overall treatment effectiveness [9,10].

Head models used for TES simulation include not only rather simple, canonical sphere models, handled both analytically and numerically, but also anatomically realistic high-resolution head models that can be handled only numerically [4]. Amongst the first attempts is the work of Rush and Driscoll [11] in which the analytical head model consisting of three concentric spheres each representing the scalp, skull and brain

* Corresponding author.

E-mail addresses: ansusnja@fesb.hr (A. Šušnjara), ozbej.verhnjak@gmail.com (O. Verhnjak), dpoljak@fesb.hr (D. Poljak), mcvetkov@fesb.hr (M. Cvetković), jure.ravnik@um.si (J. Ravnik).

tissues, is developed. Although very simple, the analytical model still serves as useful benchmark for testing more realistic representations. A convenient numerical tool used for TES simulation is the finite element method (FEM) which, in the early investigations, was applied on spherical head models, too. By varying the number of spheres, different tissues in the head were represented [12,13]. Due to improvements in human body visualisation, anatomically based models have been used in more recent studies, including the low-resolution [14,15] and high-resolution head models, respectively [5,7,16,17]. Compared to previous models the novelty proposed in this paper is a different numerical approach to deterministic solution of the TES simulation based on the Boundary Element Method (BEM), extensively used for e.g. the nanofluid flow simulations [18]. The formulation of the TES is based on a quasi-static approximation of the currents and voltages in living tissues [4]. As a first step a simple cylindrical structure is chosen for the human head model and the results are reported in [19]. The proposed technique shows a satisfactory convergence rate. Further step in modelling introduced in this paper deals with a realistic head model consisting of three layers. Note that this model is commonly used in simulations of electroencephalography and magnetoencephalography procedures, respectively, [20] and in computational high frequency dosimetry studies [21], as well.

Although deterministic numerical techniques ensure a good insight into behaviour of the underlying phenomena, there are still some issues that cannot be addressed by using solely deterministic modelling. The biological tissues represent a complex media in electromagnetic modelling and they are characterised by quantities such as permittivity, conductivity and permeability, respectively. However, the exact value of these parameters is not known, as their values may vary due to frequency, gender, age, or health of a person, respectively [10]. Most of these parameters presented in overviews such as [22] are obtained under different measurement on ex vivo animal and human tissues, and exhibit large variations from their averages [23]. When used in computational models, these average values lead to rough approximation of the real situation [24,25]. Thus, the uncertainty from the input is inevitably propagated to the output of interest which is, in this case, the scalar electric potential or the current distribution in the head tissues. Hence, these parameters need to be considered as random variables. Besides introducing the BEM approach, an additional contribution of this paper is the coupling of BEM with the stochastic collocation method (SCM) to account for the uncertainties present in the model input parameters.

At this stage it is also rather important to address the preference to use BEM over finite difference method (FDM) using this predefined regular grid – the approach often used by most of members of bioelectromagnetics society primarily because of simplicity of the approach as its main feature. On one hand, the simplicity issue in FDM seems rather attractive, but on the other hand suffers from serious drawbacks such as well-known staircasing approximation error occurring within commonly-used voxel anatomic models. This serious disadvantage in the application of FDM approaches in last few decades was recognised by Subcommittee 6 (SC6) of the IEEE International Committee on Electromagnetic Safety (ICES) on Electromagnetic field dosimetry. Within SC6 the scope of working group No 2 was to tackle with numerical artefacts. Namely, an important scope of WG2 was to study and quantify effects of numerical artefacts in low frequency (LF) dosimetry. Furthermore, specific missions were to investigate stair-casing error arising from stair-cased models, such as FDTD method and to compare them with smoothed model, such as Boundary Element Methods (BEM), and also to reduce the stair-casing error when using commonly-used voxel anatomic models. These activities included task such as comparison of domain and boundary discretisation methods, differential versus integral equation formulations thus undertaking a trade-off between the use of Scalar Potential Finite Difference (SPFD) methods, Finite Element Methods (FEM), Boundary Element Methods (BEM), use of hybrid methods, such as FEM/BEM, BEM/FDM, or combination of finite elements/infinite elements, various integral equation methods, such as volume tensor integral equations, or surface integral equations. Additional goal of WG2 was to reduce stair-

casing error when using voxel anatomic models. Studies of averaging (smoothing) of tissue parameters (pre-processing methods), averaging of calculated results (post processing methods) and application of analytical solution at singularities were of interest, as well.

In short, if one makes a trade-off between the use of FDM and conformal methods what should be emphasised is as follows:

FDM approaches

- Advantages: robustness and simplicity of the algorithm with rectangular grid rather easy to generate.
- Drawbacks: staircasing error and problems with unbounded domains.

BEM models

- Beauties: BEM definitely tends to avoid volume meshes for large-scale problems and by its nature sufficiently avoids staircasing error. BEM formulation is based on the fundamental solution of the leading operator for the governing equation thus being very competitive with other well-established methods, such as FEM or FDM, in terms of accuracy and efficiency. There is no need to implement absorbing boundary conditions (ABC) for unbounded domains. Finally, BEM provides an exact geometrical description of the problem boundary using isoparametric transformations.
- Drawbacks: BEM definitely requires a more complex formulation and related numerical implementation. Moreover, one has to sufficiently deal with Green function singularities/quasi-singularities and with dense matrices appearing in the algorithm, being computationally more expensive than FDM and FEM.

These issues have been discussed in detail in WG2 Report and in the paper arising from WG2 activities [26]. Note that TMS setup has been used in [26] and intercomparison of number of methods has been carried out including Surface integral equation (SIE)/Method of Moments (MoM), Finite Element Method (FEM) with cubical elements, Boundary Element Method (BEM), Hybrid Finite Element Method/Boundary Element Method (FEM/BEM), Finite Element Method (FEM) with rectilinear elements.

To sum up, maybe the implementation of BEM in many bioelectromagnetics problems may seem as an unnecessary complication due to the simplicity of FDM implementation, as a dominant reason why the approach has been so attractive for decades. However, if one carries out deeper numerical consideration the beauty of BEM approach due to the number of its advantages comes out as obvious fact.

In the previous work the variations of the electrodes' shape and position, as well as the size of head, the dimensions of electrodes and the cylinder were considered as random variables [19]. Here, the focus is on the material properties whose values result from an examination of a large number of studies published in the tissue properties database [27]. Hence, by means of SCM, the uncertainty is propagated to the output of interest which is the distribution of the scalar electric potential, and the corresponding stochastic mean and the variance are computed.

It is worth noting that the boundary element method (BEM) is commonly used in the modelling of electromagnetics phenomena such as ECG, MCG, EEG and MEG [28]. However, to the best of authors' knowledge the BEM applied in the area of TES simulation has not been reported in the literature so far. Authors previously performed similar analysis [29] using surface integral equation formulation [30,31], but the reported numerical approach was limited to a homogeneous brain model only. Moreover, the stochastic analysis of the transcranial electric stimulation in the available literature is scarce as well. On the other hand, the uncertainty quantification (UQ) of the fields induced in the human brain due to the exposure to coils used in TMS has been investigated to a greater extent, e.g. in [32,33], where the conductivities of brain tissues are modelled as uniformly distributed random variables and the results clearly demonstrated the importance of the

exact knowledge of the electrical conductivities in TMS. In addition to tissue conductivity, the variability of coil position and orientation and brain morphology was considered in [34,35]. Likewise, the uncertainty in the tissue parameters' values should be taken into account in the TES simulations aiming to provide reliable numerical predictions of the induced electric field, potential and current in the head tissues. One such analysis is proposed by Schimdt et al. in [36]. They investigated the impact of uncertain head tissue conductivity on optimal electrode configurations in the optimisation of tDCs suggesting that an uncertain conductivity profile can have a substantial influence on the prediction of optimal stimulation protocols for stimulation of the auditory cortex. Similarly, this contribution should be regarded as the first step in an on-going activity of applying the BEM to a realistic human head and its coupling with the SCM to account for the variability present in the electric parameters of biological tissue in the TES simulation process.

Therefore, it is worth emphasising that the goal of the coupling of SCM with BEM carried out in this paper is twofold: BEM sufficiently avoids the FDM drawbacks, such as staircasing error, while SCM accounts for the uncertainties in the input data set which is inherent problem in all bioelectromagnetics problems.

The paper is organised as follows. The formulation is presented in section II along with the description of the deterministic boundary element method. Section III outlines the approaches used for stochastic analysis, i.e. the stochastic collocation method and the analysis of variance approach for the sensitivity analysis. The computational results are given in section IV and finally some conclusions regarding the present and the on-going work are given in section.

2. Deterministic-stochastic modelling of the transcranial electric stimulation

2.1. Governing equations

The usual approach applied in modelling of a transcranial electric brain stimulation is the quasi-static approximation of voltages and currents. At low frequencies the values of electric permittivity and magnetic permeability of the biological tissues are relatively low and with a negligible variability, hence, they can be neglected. However, this is not the case with the electric conductivity [37]. Biological tissues in quasi-static approximation are considered as volume conductors in which the inductive component of the impedance is neglected, while resistances, capacitances, and voltage sources are distributed throughout a given three-dimensional domain [37]. Thus, in a typical passive volume conductor model of a biological tissue the excitability of the tissue itself is ignored and the governing equation for the electric scalar potential is the Laplace equation [4]:

$$\nabla \cdot (-\sigma \nabla \varphi) = 0 \quad (1)$$

The head model in this paper is a 3-compartment or 3-layer head model commonly used in electroencephalography and magnetoencephalography (Fig. 1). Although in the present study the emphasis is not on the particular electrode setup, the electrode position corresponds to Cz-Fpz electrode setup defined by 10/20 electroencephalogram standard for electrode placements. The electrodes in this paper are of circular shape of diameter d with the potential of ± 1 V. Hence, the boundary conditions are given as Dirichle's boundary condition $\varphi = \pm 1$ V at the circular area of the electrodes and for the rest of the domain the Neumann's boundary condition is prescribed, $-\sigma(\partial\varphi/\partial n) = 0$.

In general for an anisotropic conductor the electric conductivity is a tensor. For example, in the white matter of the brain, the electric conductivity is higher in the direction of neural fibre tracts. In this work, we model the human head as a group of subdomains representing individual tissues, which have different but homogeneous and isotropic electric conductivity. Therefore, in this case, for each subdomain, Eq. (1) simplifies to a Laplace equation:

$$\nabla^2 \varphi = 0 \quad (2)$$

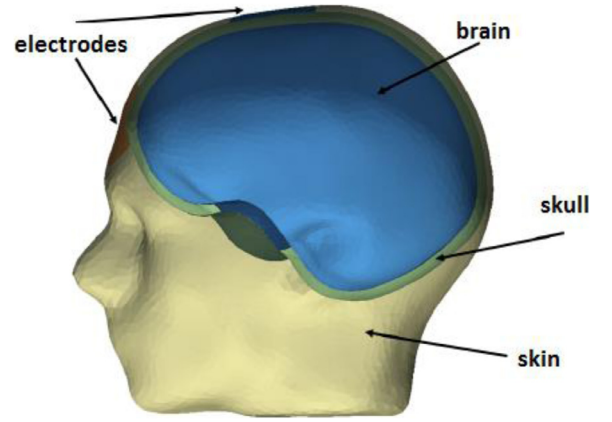


Fig. 1. A 3-layer head model.

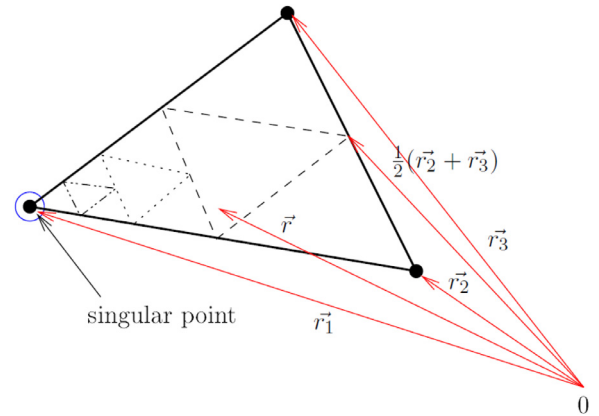


Fig. 2. Recursive subdivision of a triangle element towards the singular point.

where changes of electric conductivity between tissues are taken into account through boundary conditions.

2.2. An outline of the boundary element method

Let us consider a domain $\Omega \in R^3$ with the boundary $\Gamma = \partial\Omega$ and a location vector \vec{r} . The domain is divided into subdomains $\Omega = \sum \Omega_i$, where each subdomain has its own boundary $\Gamma_i = \partial\Omega_i$. Inside each subdomain one can write a boundary integral representation of Eq. (3) as [38]:

$$c(\vec{\xi})\varphi(\vec{\xi}) + \int_{\Gamma_i} \varphi(\vec{r}) \vec{\nabla} \varphi^* \cdot \vec{n} d\Gamma_i = \int_{\Gamma_i} \varphi^* (\vec{n} \cdot \vec{\nabla} \varphi(\vec{r})) d\Gamma_i, \quad \vec{\xi} \in \Gamma_i \quad (3)$$

where Γ_i is the boundary of i -th subdomain, $\vec{\xi}$ is the source point, c is the free coefficient, and $\varphi^* = 1 / 4\pi |\vec{r} - \vec{\xi}|$ is the fundamental solution of the Laplace operator. Such a representation enables us to only solve for the unknowns at the boundary of the subdomain, since the solution in the interior depends only of the knowledge of boundary variables (potential $\varphi(\vec{r})$ and flux $q = \vec{n} \cdot \vec{\nabla} \varphi(\vec{r})$).

In order to obtain a system of linear equations for the unknowns at the boundary subdomain boundaries are discretised using triangular elements. Within triangles we use linear interpolation of potential $\varphi(\vec{r}) = \sum \varphi_j(\vec{r})$ and constant interpolation of flux. Using this interpolation scheme one must calculate the following integrals, which are stored in matrices $[H_i]$ and $[G_i]$:

$$[H_i] = \int_{\Gamma_i} \Phi_j \vec{\nabla} \varphi^* \cdot \vec{n} d\Gamma_i, \quad [G_i] = \int_{\Gamma_i} \varphi^* d\Gamma_i, \quad (4)$$

Thus, for each subdomain, a system of linear equations is obtained:

$$c_i \varphi + [H_i] \{\varphi\} = [G_i] \{q\} \quad (5)$$

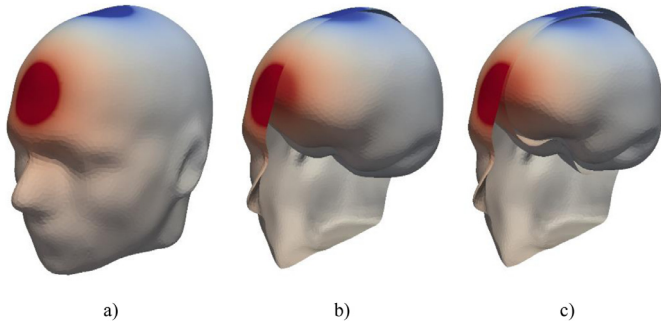


Fig. 3. Distribution of electric potential on the surface of skin (a), skull (b) and brain (c) in a 3-layer head model.

where $\{\varphi\}$ and $\{q\}$ are vectors of nodal values of potential and flux. Calculation of the free coefficient $c(\vec{x})$ and the strongly singular diagonal element of $[H_i]$ is performed indirectly. Setting $\varphi=1, q=0$ as one of the valid solutions of the original problem, we can use Eq. (5) to evaluate the sum of c and the diagonal element in the $[H_i]$ matrix, when all other elements have been evaluated beforehand using numerical integration.

Integrals in Eq. (4) are calculated numerically over triangles in 3D space. Research into numerical integration over triangulated surfaces has been ongoing for many decades [39,40], since it is needed in BEM as well as by other numerical methods. One of the ideas proposed is the idea of using domain decomposition to improve accuracy of integration schemes [41]. Precision of calculation of any integral over any domain

can be improved by dividing the domain into smaller subdomains, which are integrated separately. In case of singular integrals, such as we encounter in BEM, it makes sense to make subdomains small in the area around the singular point. In this paper, we propose a recursive scheme to achieve this, which is described below.

For the purpose of linear interpolation within each triangle it is convenient to use barycentric coordinate system $(\lambda_1, \lambda_2, \lambda_3)$. A position within a triangle is then calculated by $\vec{r} = \lambda_1\vec{r}_1 + \lambda_2\vec{r}_2 + \lambda_3\vec{r}_3$. Weights and integration point locations were taken out of [42] and converted to the barycentric coordinate system. We obtained lists of $(w_i, \lambda_{1i}, \lambda_{2i}, \lambda_{3i})$ with 7, 25, 54, 85 and 126 entries, which provide machine precision accurate integration of polynomials of degree 5, 10, 15, 20 and 25 respectively. With this, integral over a triangle τ can be approximated by

$$\int_{\tau} f(\vec{r}) d\Gamma \approx \sum_i w_i f(\lambda_{1,i}\vec{r}_1 + \lambda_{2,i}\vec{r}_2 + \lambda_{3,i}\vec{r}_3) \quad (6)$$

When using the boundary element method, we are faced with the calculation of singular integrals. The singularity is placed in one of the vertexes of the triangle (for linear interpolation schemes) or in the barycentre of the triangle (for constant interpolation scheme). In order to accurately calculate such integrals, we used a recursive subdivision of the triangle towards the singular point. Fig. 2 demonstrates the recursive algorithm. In each step the triangle is subdivided into four smaller triangles, which are obtained by halving the triangle sides. The one small triangle, which still includes the singularity, is divided again in the next step. The number of parts into which the triangle is divided is $1 + 3n$, where n is the number of recursive steps. The final results is a sum of integrals calculated on all parts. The number of recursive

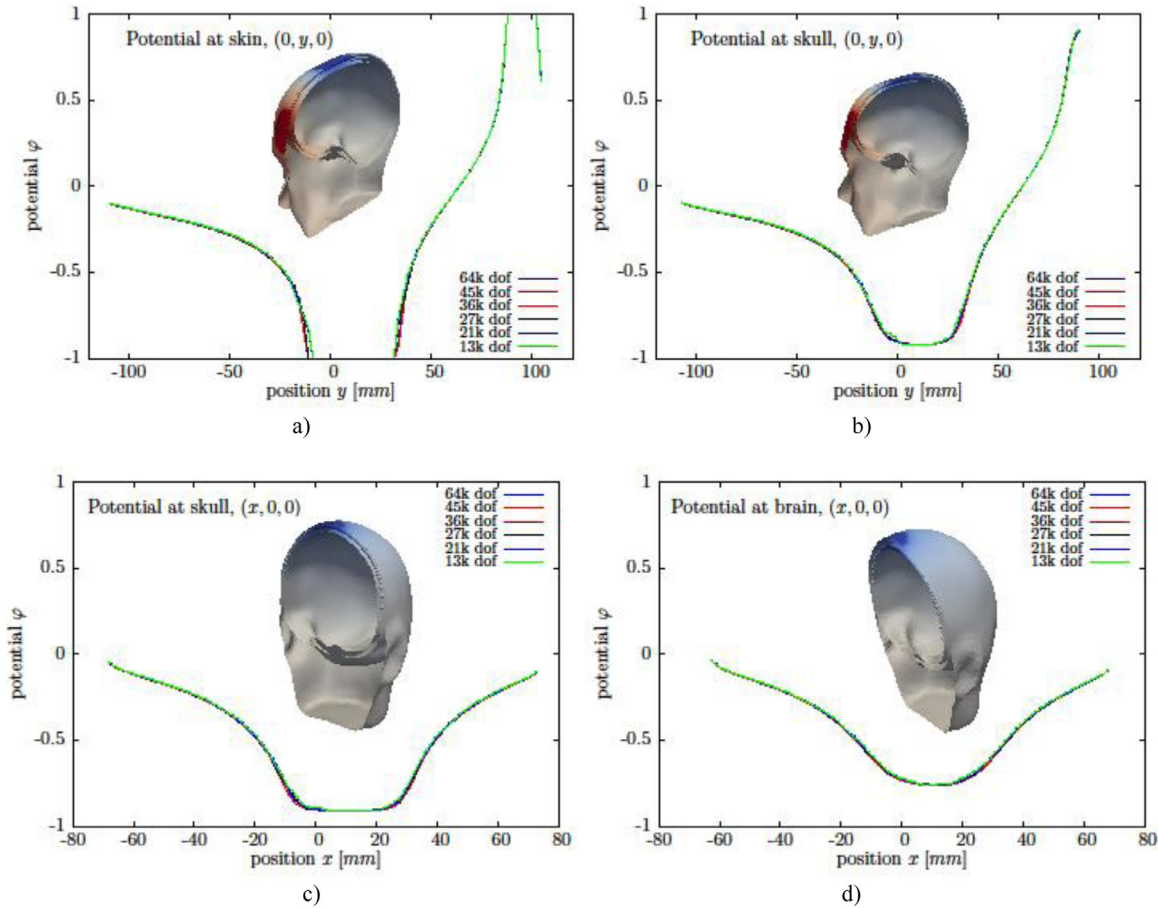


Fig. 4. Computational grid analysis for 3-layer head model.

Distribution of electric scalar potential is given at two profiles: $(x, 0, 0)$ and $(0, y, 0)$ for skull (b,c), skin (a) and brain (c). By changing degrees of freedom from 13k to 64k, potential values exhibit a negligible difference which points out the independence of the computational grid.

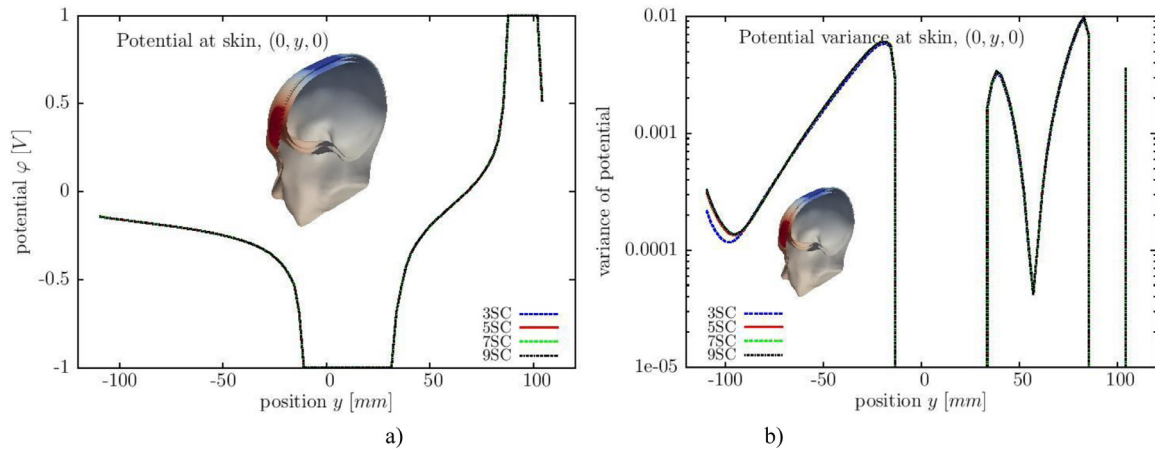


Fig. 5. Distribution of scalar electric potential along y axis for fixed $(x,z) = (0,0)$ point at skin surface: Mean (a) and variance (b) values obtained with different number of stochastic collocation points.

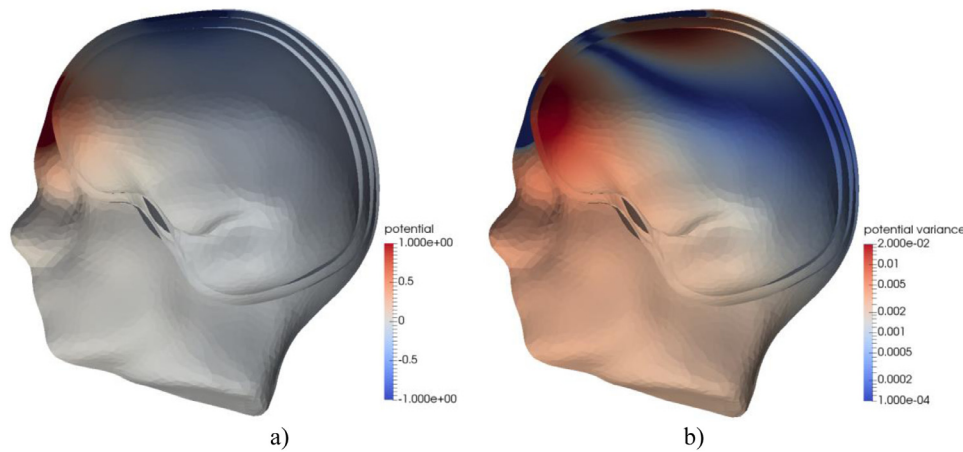


Fig. 6. The distribution of the mean (a) and variance (b) values for the electric potential in the head tissues.

steps controls the accuracy and can be adjusted to match the accuracy of calculation of non-singular integrals.

By placing the source point in all boundary potential and flux nodes in all boundaries of all subdomains, we obtain an overdetermined system of linear equations (since nodes are shared between subdomains). At the boundaries between continuity of potential and conservation of current are prescribed, while at the outer boundary either known potential or known current are specified. The resulting system of linear equations is solved for unknown potential and current using a least-squares based solver [43]. An alternative approach has been proposed by Loeffler and Mansour who instead of domain decomposition use domain superposition [44].

3. Methods for the stochastic analysis

3.1. Uncertainty quantification

Once the deterministic modelling of a problem of interest is completed, a stochastic analysis of the numerical results can be carried out via the non-intrusive uncertainty propagation methods. The main reason for choosing the non-intrusive approach is the fact that previously validated computational models, such as the BEM model outlined in the Section 2, can be used without changing the existing codes. This is a very important feature in the area of computational bioelectromagnetism as the formulation of the problem involves equations that are not easily dealt with by intrusive stochastic methods. Namely, such methods eventually lead to rather complex and tedious numerical codes being computationally very demanding. Therefore, in this paper a stochastic

collocation method (SCM) is chosen to carry out the uncertainty propagation. The deterministic code is run at discrete number of input points and uncertainty quantification is merely a stochastic post processing of the set of input points. Though this is a standard procedure used in Monte Carlo simulations [45], an important difference is that the input points are chosen in a “smart” way by following strong mathematical background and polynomial representation of the stochastic output [46]. The details of SCM have been addressed in [47] where the same head model has been used for internal field stochastic dosimetry. In that work an efficient coupling between the stochastic collocation and a hybrid boundary element/ finite element method is presented.

For the sake of completeness the expressions for the moments are outlined. The mean and variance are computed by using the following formulas:

$$\mu(Y(\xi)) \approx \sum_{i=1}^N Y^{(i)} w_i \tag{7.a}$$

$$Var(Y) \approx \sum_{i=1}^N (Y^{(i)})^2 w_i - \mu^2 \tag{7.b}$$

where $Y^{(i)}$ corresponds to i th simulation of deterministic code, N is the total number of simulation points and w_i is the weight of simulation point defined by the following integral:

$$w_i = \int_{\Gamma} L_i(X) p(X) dX \tag{8}$$

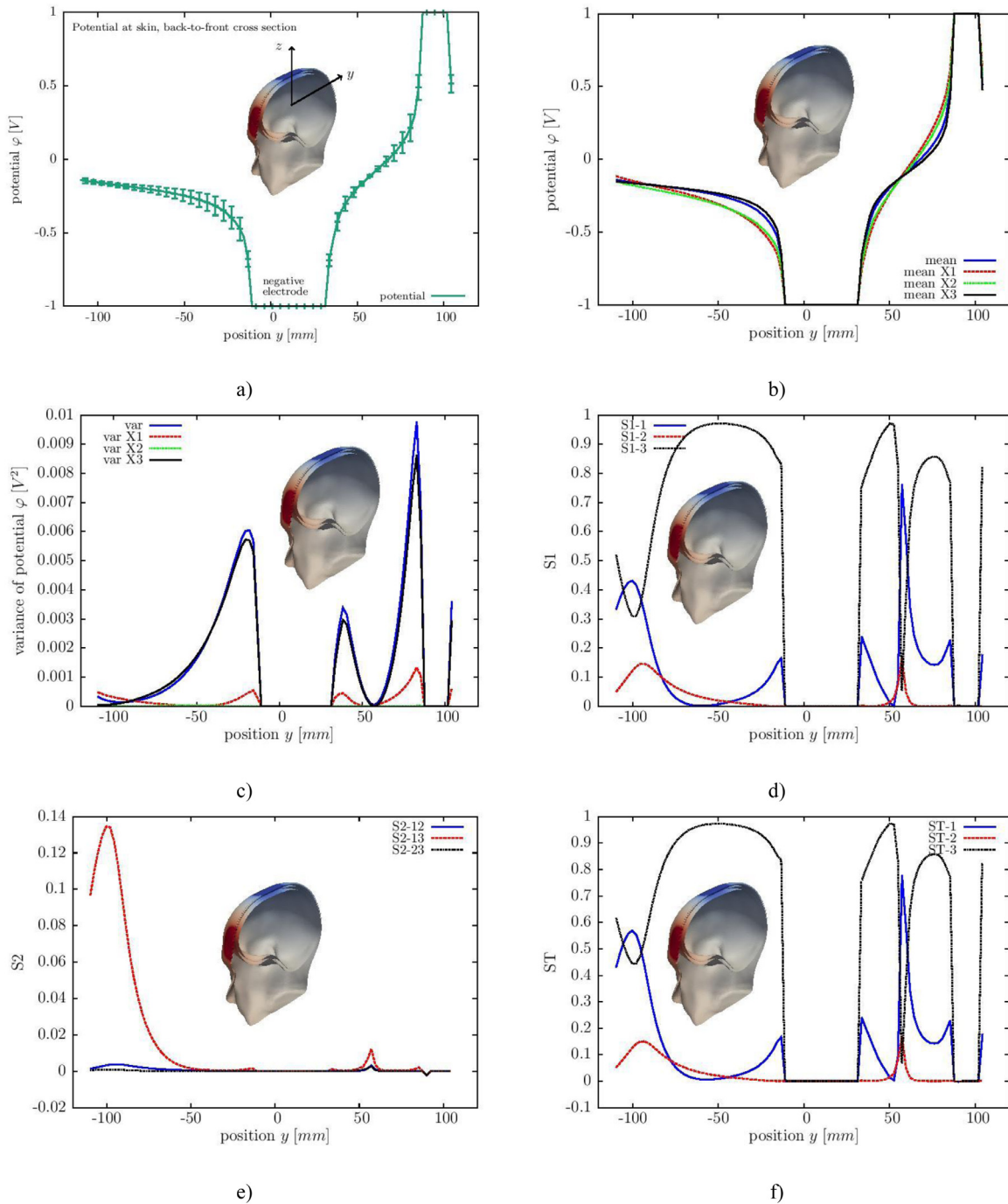


Fig. 7. Distribution of scalar electric potential along y axis for fixed $(x,z)=(0,0)$ point at skin: a) mean +/- standard deviation; b) mean and c) variance values for cases $\mathbf{X} = [X_1 X_2 X_3]$, $\mathbf{X} = [X_1]$, $\mathbf{X} = [X_2]$ and $\mathbf{X} = [X_3]$; Sensitivity indices: d) $S1$, the 1st order; e) $S2$, the 2nd order and f) ST , total effect.

$L_i(\mathbf{X})$ in the Eq. (8) is the multivariate basis function used for the polynomial approximation of the output $Y(\mathbf{X})$ while $p(\mathbf{X})$ is the joint probability density function of input parameters which are organised in the vector $\mathbf{X} = [X_1, X_2, \dots, X_d]$ [47].

Stochastic collocation comes in different variants depending on the choice of basis functions $L_i(\mathbf{X})$ and appropriate integration rule for solving the integral in Eq. (8). In this work the Gauss integration rule and Lagrange interpolation are used, while multidimensional integration is carried out using the tensor product.

3.2. Sensitivity analysis

In addition to uncertainty quantification, the sensitivity analysis (SA) is often carried out for models whose input parameters exhibit random nature. One of the definitions for the SA, adopted in this work as well, is the one describing it as the study of how the uncertainty in the output of a mathematical model or system (numerical or otherwise) can be apportioned to different sources of uncertainty in its inputs [48]. The ideal approach would be to run both uncertainty quantification and sensitivity

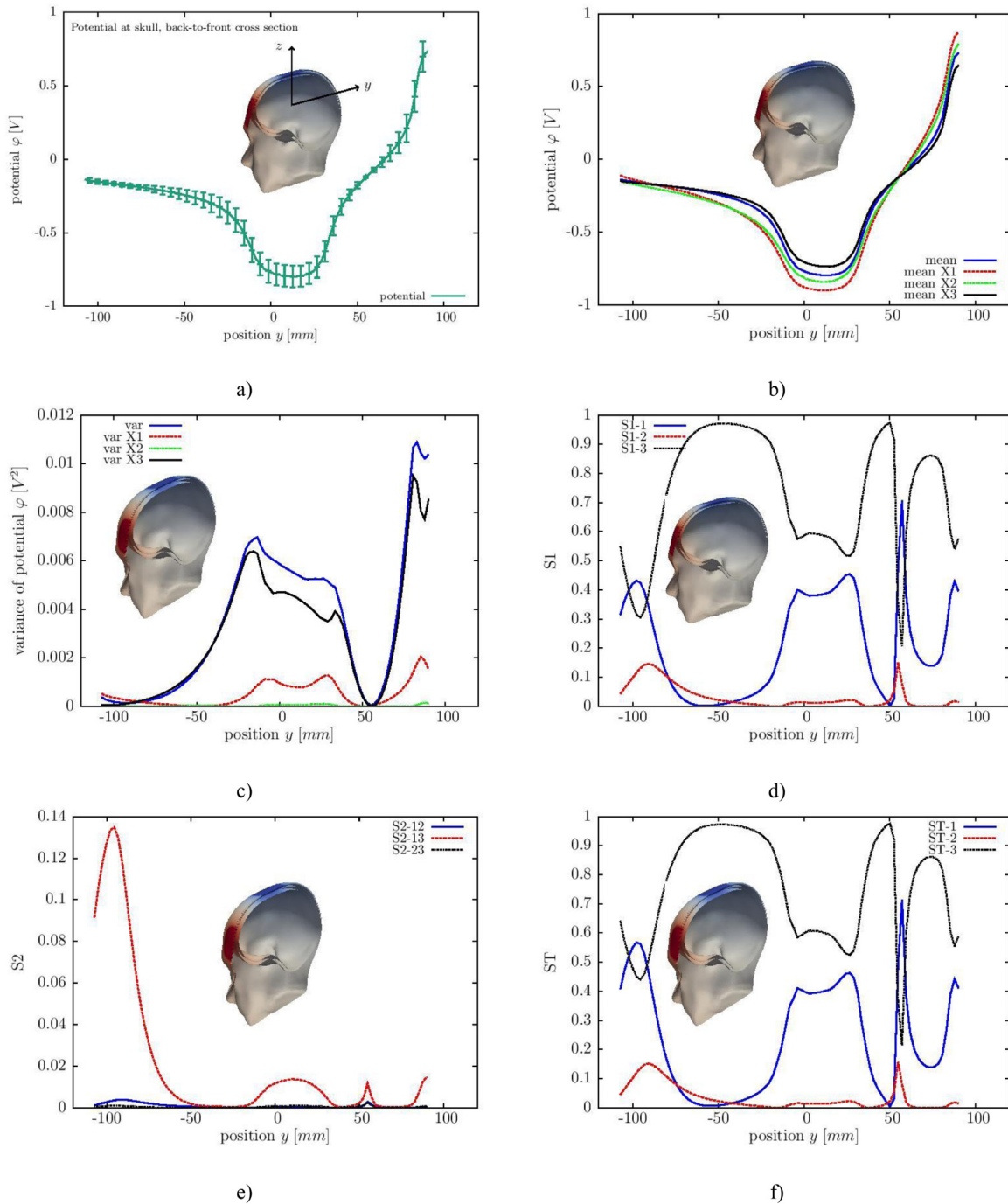


Fig. 8. Distribution of scalar electric potential along y axis for fixed $(x,z)=(0,0)$ point at skin: a) mean +/- standard deviation; b) mean and c) variance values for cases $\mathbf{X} = [X_1 X_2 X_3]$, $\mathbf{X} = [X_1]$, $\mathbf{X} = [X_2]$ and $\mathbf{X} = [X_3]$; Sensitivity indices: d) $S1$, the 1st order; e) $S2$, the 2nd order and f) ST , total effect.

analysis in the same stochastic framework, usually UQ preceding the SA, thus minimising the computational burden as much as possible [49]. In this work we use the stochastic collocation both for UQ and SA. The conducted SA here relies on two approaches: the so-called “one-at-a-time” approach and the approach based on the variance analysis. The details pertaining to each of the approaches have been carried out in the [47]. Here, only the final formula and the definitions are given for the sake of completeness.

3.2.1. One-at-a-time approach, OAT

Within the stochastic framework used in this work the sensitivity is estimated by monitoring the change in the variance of the output after computing the variance for d univariate cases and simply comparing the variances of the output value for each univariate case [47].

3.2.2. The Analysis Of VAriance approach, ANOVA

In order to take into account the simultaneous variation of input variables the Analysis of Variance (ANOVA) approach originating from

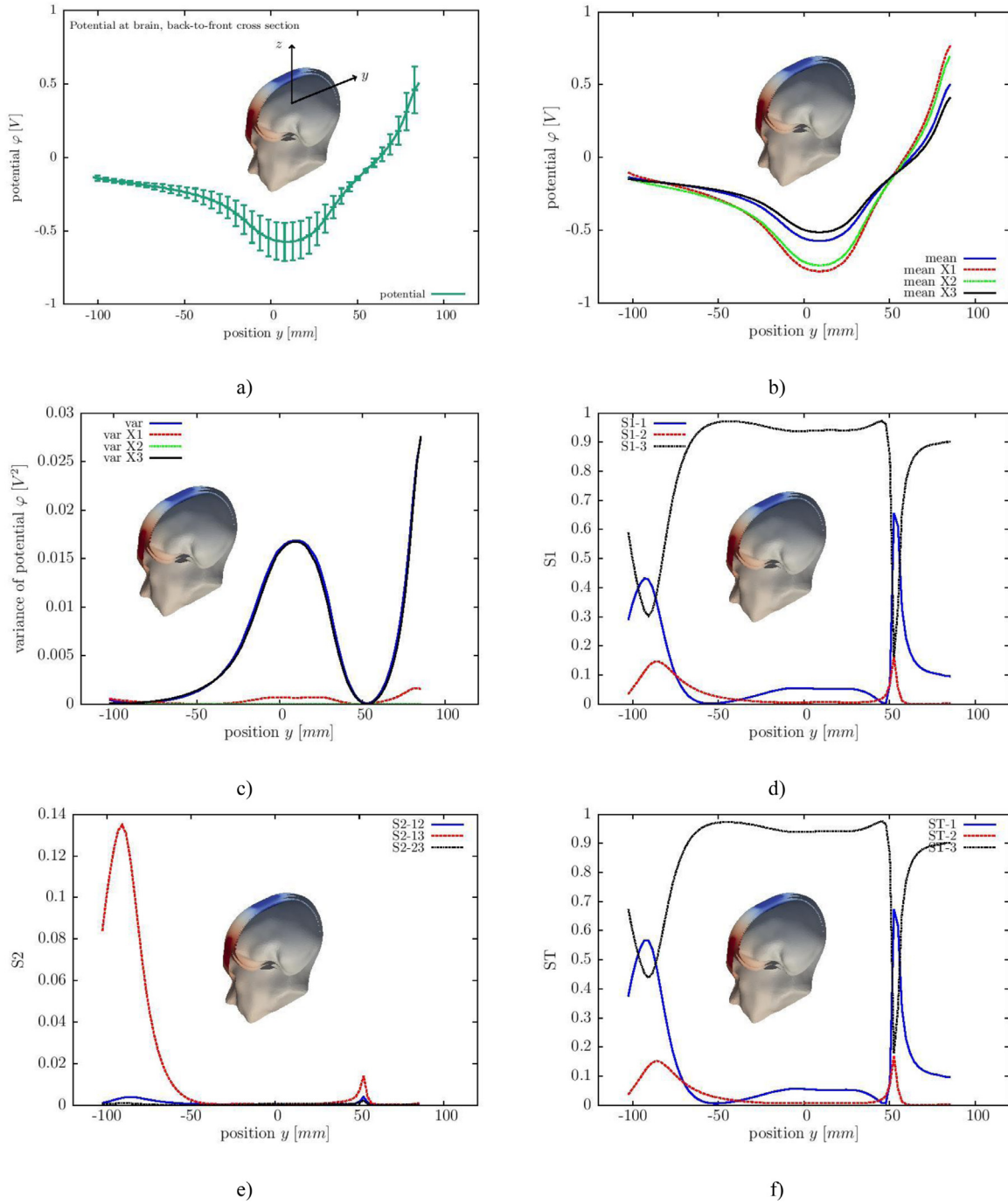


Fig. 9. Distribution of scalar electric potential along y axis for fixed $(x,z)=(0,0)$ point at **brain**:

- a) mean +/- standard deviation;
- b) mean and c) variance values for cases $\mathbf{X} = [X_1 X_2 X_3]$, $\mathbf{X} = [X_1]$, $\mathbf{X} = [X_2]$ and $\mathbf{X} = [X_3]$;
- Sensitivity indices: d) $S1$, the 1st order; e) $S2$, the 2nd order and f) ST , total effect.

the work of Sobol [50] is here used as well. The detailed description is given in [47], while here only the final expressions are repeated. Hence, the first order sensitivity indices $S1$ measure the effect of only the k -th random input variable, without any interaction with other RVs. The 1st order sensitivity index is given by the following expression:

$$S1_k = \frac{V_k}{V(Y)}, \quad k = 1, \dots, d \tag{9}$$

where $V(Y)$ is the variance of the D -dimensional case while V_k is the variance of the k -th 1-dimensional case.

The second and high order sensitivity indices, $S2_{ij}$ and $S_{d12,\dots,d}$ give the information about the effect that the interaction of two, three or more random input variables has w.r.t. to the output. E.g. the 2nd order sensitivity index is given by the following expression:

$$S2_{ij} = \frac{V_{ij}}{V(Y)}, \quad i = 1, \dots, d; \quad j > i \tag{10}$$

where $V_{ij} = V(f_{ij}(X_i, X_j))$ is the conditional variance whose expression is defined in [47] and the meaning is: the variance that originates from the mutual interaction between the i th and j -th input parameter.

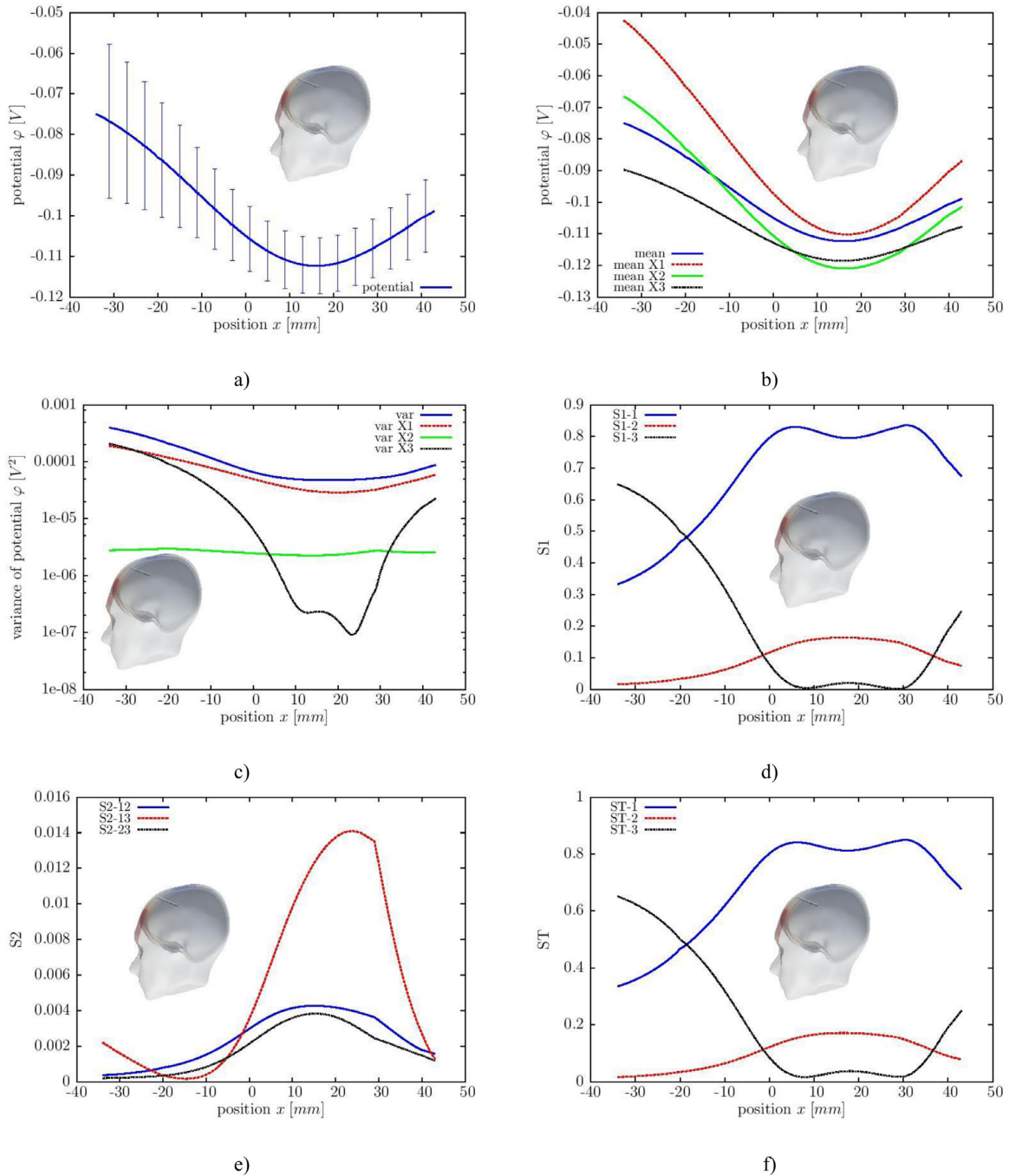


Fig. 10. Distribution of scalar electric potential along x axis for fixed $(y,z)=(50\text{ mm},90\text{ mm})$:
 a) mean +/- standard deviation;
 b) mean and c) variance values for cases $\mathbf{X} = [X_1\ X_2\ X_3]$, $\mathbf{X} = [X_1]$, $\mathbf{X} = [X_2]$ and $\mathbf{X} = [X_3]$;
 Sensitivity indices: d) SI_1 , the 1st order; e) $S2$, the 2nd order and f) ST , total effect.

Finally, the computational burden may become very prohibitive when all groups of sensitivity indices needs to be computed, therefore, very often only the 1st order sensitivity index is computed. In order to still obtain the information about the potential significant interactions between the variables, a total effect sensitivity index is defined as:

$$ST_k = \frac{E_{X_{\sim k}}[V_{X_k}(Y|X_{\sim k})]}{V(Y)}, \quad k = 1, \dots, d \tag{11}$$

The total effect index measures the contribution to the output variance of X_k , including all variance caused by its interactions, of any

order, with any other input variables. Here E denotes the expected value operator and notation tilde (\sim) denotes all but operator, i.e. $E_{X_{\sim k}}(Y|X_k)$ means the expected value of V calculated by varying all input variables except X_k .

3.3. Numerical results

The value for the conductivity of the three tissues is chosen based on the examination of a large number of studies published in the tissue properties database [27]. The conductivities of brain and skin are modelled as random variables uniformly distributed between the

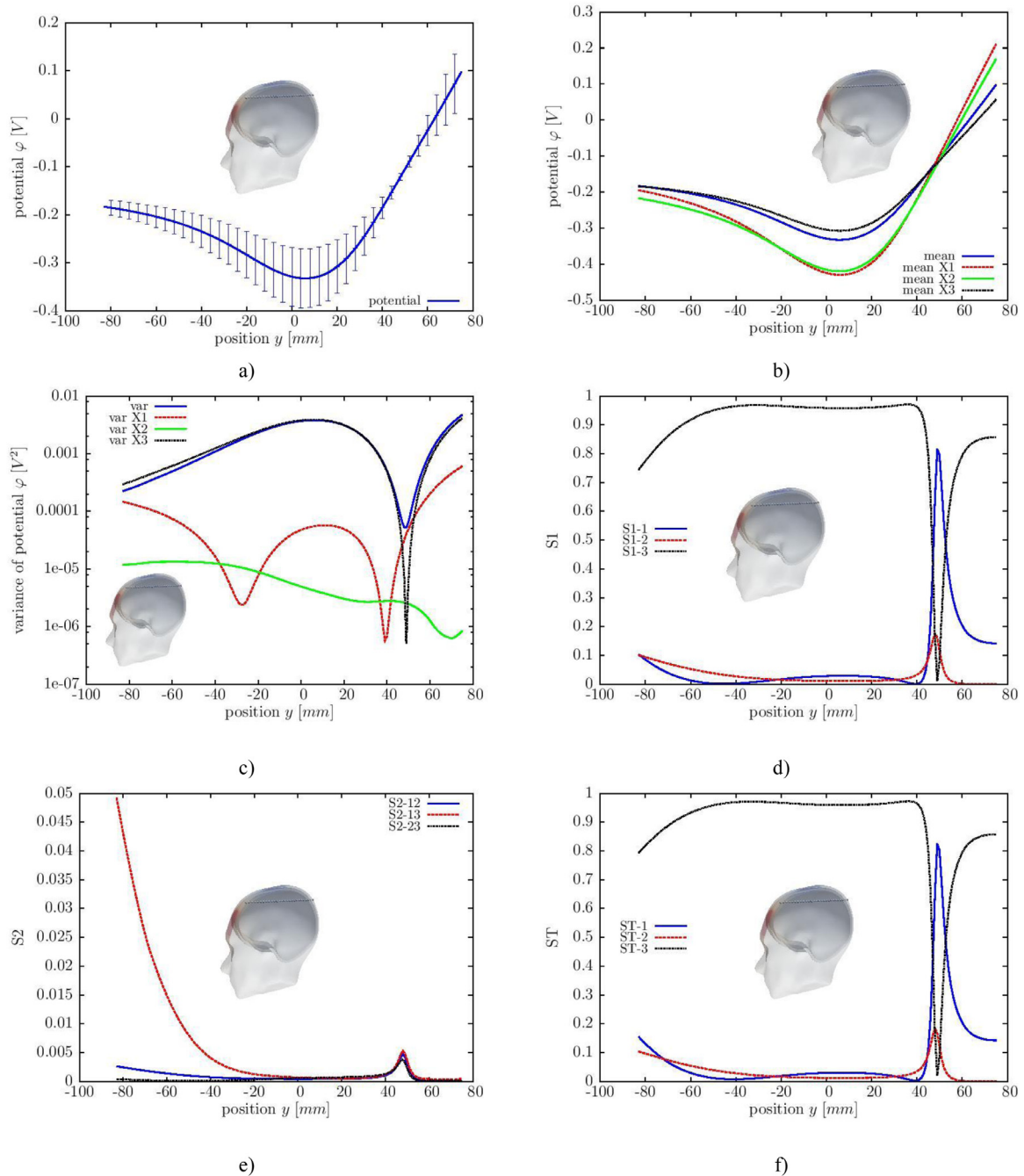


Fig. 11. Distribution of scalar electric potential along y axis for fixed $(x,z)=(0\text{ mm},90\text{ mm})$:
 a) mean +/- standard deviation;
 b) mean and c) variance values for cases $\mathbf{X} = [X_1\ X_2\ X_3]$, $\mathbf{X} = [X_1]$, $\mathbf{X} = [X_2]$ and $\mathbf{X} = [X_3]$;
 Sensitivity indices: d) $S1$, the 1st order; e) $S2$, the 2nd order and f) ST , total effect.

minimal and maximal reported values. Since only one study measured the skull conductivity we considered 20% uniform distribution around the published average value. The conductivities for all three tissues are given in Table 1.

The distribution of the electric potential when all tissues have average value of their respective conductivity is depicted in Fig. 3. The electrode voltage is +/- 1 V (the red and the blue circular areas). The results could be scaled to a different values of applied electrode voltages.

Table 1
 The values for the tissue conductivities.

Tissue name	σ_{\min} (S/m)	σ_{\max} (S/m)
Skin	0.09	0.25
Skull (bone cortical)	0.256	0.384
Brain (bold + white matter)	0.0644	1.28

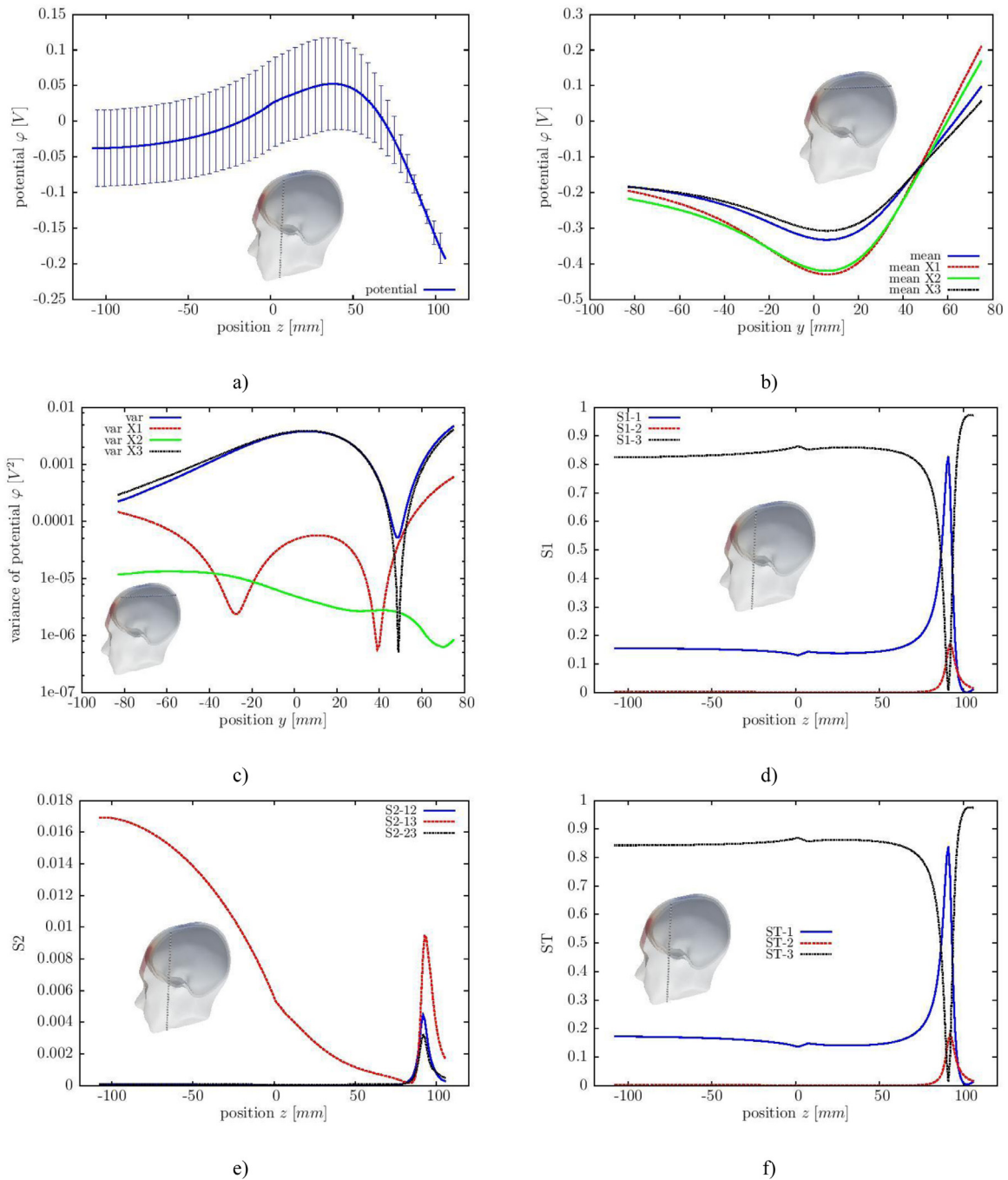


Fig. 12. Distribution of scalar electric potential along z axis for fixed $(x,y)=(0\text{ mm},50\text{ mm})$:
 a) mean +/- standard deviation;
 b) mean and c) variance values for cases $\mathbf{X} = [X_1\ X_2\ X_3]$, $\mathbf{X} = [X_1]$, $\mathbf{X} = [X_2]$ and $\mathbf{X} = [X_3]$;
 Sensitivity indices: d) $S1$, the 1st order; e) $S2$, the 2nd order and f) ST , total effect.

3.3.1. Computational mesh analysis and convergence

In order to ensure that the simulation results are grid independent, several computational grids are prepared having between 13 and 64 thousand degrees of freedom (dof). Comparison of potential profiles on different parts of the model are shown in Fig. 4. Only very small differences between results can be observed, thus the 36 thousand dof mesh is chosen for the further analysis. To ensure the highest possible accuracy of deterministic simulations, a double precision is used and the solver stopping criterion of 10^{-15} . The reason of choosing such a strict stopping criterion is to minimise the numerical error as much possible in order to better expose the physical sources of uncertainty. The deter-

ministic solver capable of solving the Laplace equation on subdomains with different conductivities has been developed in-house using Fortran.

3.3.2. Stochastic analysis

In order to check the convergence of the stochastic collocation method the design of experiment (DoE) was built by using 3, 5, 7 and 9 collocation points in each dimension, thus resulting in 27, 125, 343 and 729 deterministic simulations. The distribution of the mean and the variance of the electric scalar potential distribution along some points in the head model for different level of SC accuracy is shown in the Fig. 5. The convergence of the stochastic approach is accomplished

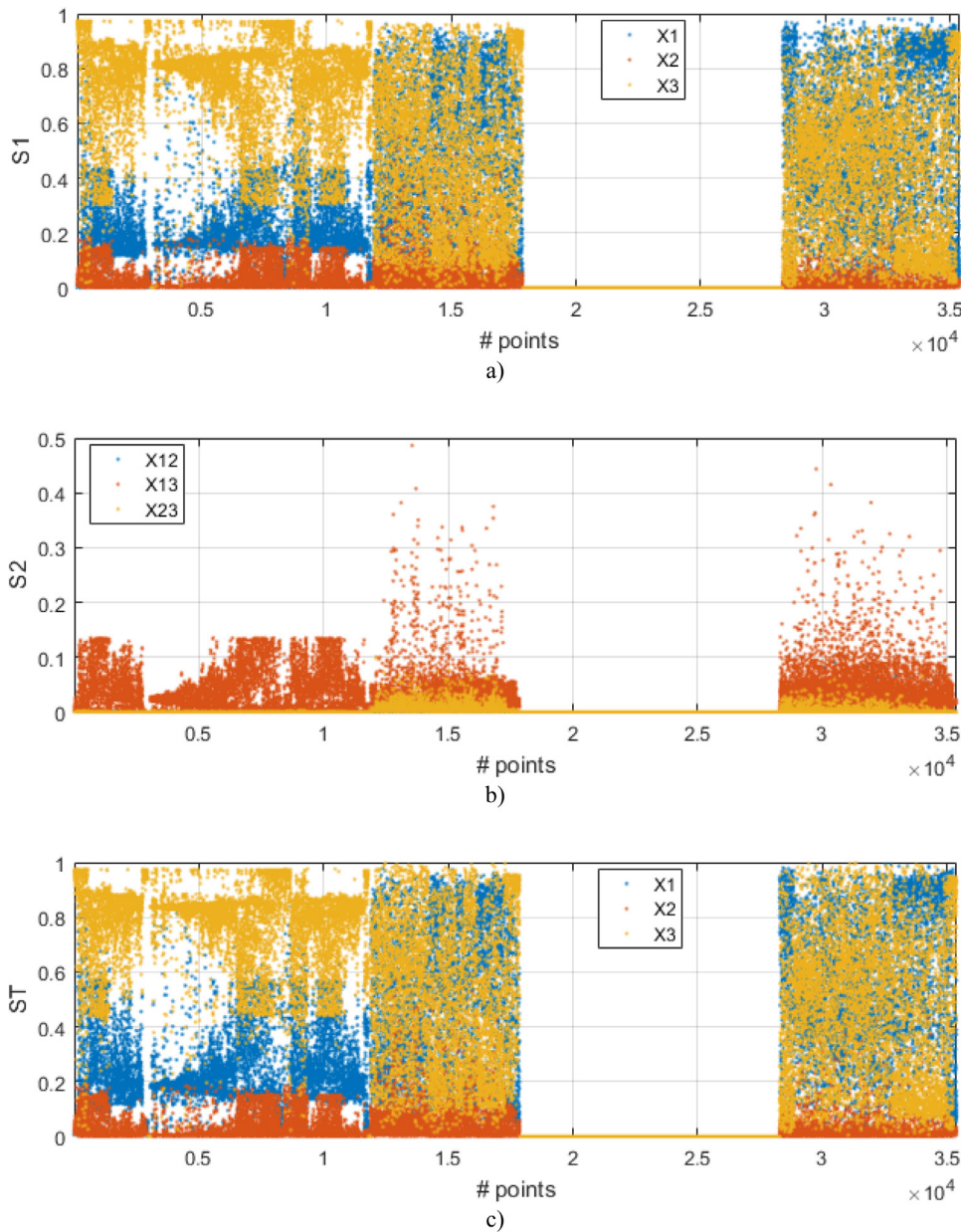


Fig. 13. The 1st (a), the 2nd (b) order sensitivity indices and the total effect (c) sensitivity indices at every point of computation. X1, X2 and X3 are the conductivities of scalp, skull and brain, respectively. The X12, X13 and X23 stand for the mutual interaction between the tissue conductivities. 1, 2 and 3 stand for the head, skull and scalp tissues.

with 3 SC points in case of the stochastic mean, while 5 SC points is enough for the computation of the stochastic variance of the output electric scalar potential. The distribution of the stochastic mean and the variance at the surface of the head tissues is depicted in the Fig. 6.

The results in the Figs. 7–12 are presented in the following way: each figure has three rows and two columns which leads to six parts in total (a-f). The meaning of these six parts is covered in the following text along with the discussion.

The top left part (a) in Figs. 7–12 presents the distribution of the mean value of the electric scalar potential along with the confidence intervals (CI). The confidence intervals are obtained as the mean \pm one standard deviation, computed as the square root of the variance. Observing this graph for all of the figures it can be concluded that the confidence margins are larger as the observation points move towards the interior tissue. When comparing Figs. 7a, 8a and 9a the CI increase as we move from 7a to 9a. Even if each of those figures is observed independently it is clear that the spread of potential values around its mean is larger in the middle part of graph and reduces towards the end. Figs. 10a, 11a and 12a show different profiles, but the trend is the

same: the CI gets narrower towards the exterior part. This means that the values of scalar potential in the interior parts depend more on better knowledge of tissue properties than it is the case with the exterior part.

Furthermore, the top right part (b) in Figs. 7–12 shows the mean value of the scalar electric potential for three univariate cases, $\mathbf{X} = [X_1]$, $\mathbf{X} = [X_2]$ and $\mathbf{X} = [X_3]$ and for one 3-variate case, $\mathbf{X} = [X_1 X_2 X_3]$. The variables X_1 , X_2 and X_3 correspond to the conductivities σ_1 , σ_2 and σ_3 , and numbers 1, 2 and 3 denote the tissues: skin, skull and brain, respectively. The mean value observed for the $\mathbf{X} = [X_3]$ is similar to the mean in case when $\mathbf{X} = [X_1 X_2 X_3]$.

The parts denoted with (c) in Figs. 7–12 show the distribution of the variance of the electric potential for three univariate cases, $\mathbf{X} = [X_1]$, $\mathbf{X} = [X_2]$ and $\mathbf{X} = [X_3]$ as well as for the 3-variate case, $\mathbf{X} = [X_1 X_2 X_3]$. This figure corresponds to the OAT sensitivity analysis approach. The variance of the results in case of $\mathbf{X} = [X_3]$ is almost identical to the total variance in 3-dimensional case for most of the chosen profiles which indicates that the variable X_3 , i.e. the conductivity of the brain σ_3 , is the most influential variable in the input space. Inspecting the part c) in Figs. 7–9 it could be concluded that the brain conductivity is the

biggest source of uncertainty for the potential values in all three tissues. However, this is not the case for all of the observation points as it can be seen in Fig. 10. There a different profile is chosen which means that the observation points set is changed. Here the skin conductivity has the main impact and for some observation points the impact of brain conductivity is lower than the impact of the skull conductivity.

In order to get more accurate SA results, the ANOVA approach is carried out which is depicted in parts (d, e, f) of the Figs. 7–12. Namely, the 1st order sensitivity indices are depicted in (d), the 2nd order in (e) and total effect indices are given part (f). The 1st order sensitivity index is the highest for the third variable (brain conductivity) which makes it the most influential one at most of the observation points. The influence of the first variable, i.e. skin conductivity shouldn't be neglected while the impact of the second variable, i.e. the skull conductivity is the weakest, although at some points it does approach the 20% of the total impact. The magnitude of the 2nd order sensitivity index ($S2-12$, $S2-13$, $S2-23$) is not very high but the interaction of the variables X_1 and X_3 ($S2-13$) should be investigated because the impact of their mutual interaction is sometimes higher than 10%. Since the 2nd order sensitivity index is not very big the total effect sensitivity index ($ST-1$, $ST-2$, $ST-3$) is almost identical to the first order sensitivity index for each input variable.

The ANOVA SA for every computation point of interest is further depicted in the Fig. 13. The overall dominance of the brain conductivity is obvious, but the importance of taking into account of the variability in the value of the skin conductivity is visible for some of the points. Also, in minor part of the computation domain the impact of the mutual interaction of the skin and brain conductivities has a very high impact on total variance of the resulting electric scalar potential.

4. Discussion

This paper proposes the stochastic-deterministic method for simulation of the transcranial electric stimulation. The proposed approach is a combination of boundary element method (BEM) which serves as a deterministic solver and the stochastic collocation method (SCM) applied as a wrapper around it to assess the uncertainty quantification of the output of interest. The human head is represented by three layers: skin, skull and brain tissues, respectively. Tissue conductivities are considered as random variables uniformly distributed in ranges taken from the relevant literature and tissue properties databases.

The convergence of BEM is satisfactory: several computational grids are tested having between 13 and 64 thousand degrees of freedom. Comparison of potential profiles on different parts of the model show that only very small differences between results can be observed and that the simulation results are grid independent. For example, in [36] FEM was applied to a 4 layer TES model (skin, skull, white and grey matter) resulting in 2.2 million degrees of freedom (dof) with a residual error of 10^{-7} and 80 min of simulation time while in [7] the 4 layer TES model (consisting of brain, CSF, skull and scalp) resulted in 52,981 nodes and 330,789 elements. In our work up to 64k dof are located on the boundary of four subdomains. On the other hand the FEM code requires discretisation of the whole domain, thus a much larger number of dof is needed. The results on Fig. 4 show the grid independency thus exposing the main advantage of BEM over FEM in this case. This is extremely important for further stochastic analysis since a lot of deterministic simulations are needed and it is imperative that the CPU time requirements for a single simulation run are as short as possible. We believe that the effort needed to solve the 36k full matrix system of linear equations is smaller compared to 2.2 million dof sparse system. Our deterministic simulation required 45 min per run at solver accuracy 10^{-15} . In addition, it is easier to produce 2D surface meshes of complex domains, such as the human brain, as compared to volume meshes required by FEM.

Furthermore, the stochastic collocation method has been applied for the Design of Experiment with different number of SC points. The convergence of the stochastic approach has been accomplished even for the 3SC points in each dimension for stochastic mean, while 5 SC

points were enough for variance. This led to a choice of 5SC points in each dimension and a total of 125 deterministic simulations which are necessary for the stochastic analysis. This number is relatively low and can be compared to a total of 465 deterministic simulations reported for a 4-layer model in [36].

To sum up, the coupling of the BEM and SCM is proven to be successful providing an efficient tool for stochastic analysis of output values in the simulation of TES. The mean and the variance values of the electric scalar potential in the head tissues are computed and the results indicate that the confidence intervals are larger in the interior tissues, being the largest in the brain tissue. The sensitivity analysis based on the ANalysis Of VAriance approach has been carried out showing that the brain and skin conductivities have a significant impact on the variability of the resulting electric potential while the impact of skull conductivity could be neglected and excluded as the source of uncertainty in the future studies since its impact is rather low at most of the observation points.

Next step is a stochastic-deterministic analysis of a 9-layer head model consisting of skin, skull, jaw, tongue, ventricles, grey matter, white matter, cerebellum and cerebrospinal fluid (CSF). Also, different electrode set up is going to be investigated.

Declaration of Competing Interest

None.

Acknowledgement

This work was supported by the Croatian Ministry of science, education and sports and Slovenian Research Agency (research core funding No. P2-0196 and bilateral agreement BI-HR/18-19-010)

References

- [1] Kadosh ERC. The stimulated brain. Elsevier; 2014.
- [2] Woods AJ. A technical guide to tDCS, and related non-invasive brain stimulation tools. Clin Neurophysiol 2016;127(2):1031–48.
- [3] Johnson MD, Lim HH, Netoff TI, Connolly AT, Johnson N, Roy A, Holt A, Lim KO, Carey JR, Vitek JL, He B. Neuromodulation for brain disorders: challenges and opportunities. IEEE Trans Biomed Eng 2013;60(3):610–24.
- [4] Bai S, Loo C, Dokos S. A review of computational models of transcranial electrical stimulation. Crit Rev Biomed Eng 2013;41(1):21–35.
- [5] Noetscher GM, Yanamadala J, Makarov SN, Pascual-Leone A. Comparison of cephalic and extracephalic montages for transcranial direct current stimulation—a numerical study. IEEE Trans Biomed Eng 2014;61(9):2488–98.
- [6] Kwon OI, Sajib SZ, Sersa I, Oh TI, Jeong W, Kim HJ, Woo EJ. Current density imaging during transcranial direct current stimulation using DT-MRI and MREIT: algorithm development and numerical simulations. IEEE Trans Biomed Eng 2016;63(1):168–75.
- [7] Lee C, Kim E, Im CK. Techniques for efficient computation of electric fields generated by transcranial direct-current stimulation. IEEE Trans Magn 2018;54(5):1–5.
- [8] Horvath JC, Carter O, Forte JD. Transcranial direct current stimulation: five important issues we aren't discussing (but probably should be). Front Syst Neurosci 2014;8(2):1–8.
- [9] Parazzini M, Fiochi S, Cancelli A, Cottone C, Liorni I, Ravazzani P, Tecchio F. A computational model of the electric field distribution due to regional personalized or nonpersonalized electrodes to select transcranial electric stimulation target. IEEE Trans Biomed Eng 2017;64(1):184–95.
- [10] Laakso I, Tanaka S, Koyama S, De Santis V, Hirata A. Inter-subject variability in electric fields of motor cortical tDCS. Brain Stimul 2015;8(5):906–13.
- [11] Rush S, Driscoll DA. Current distribution in the brain from surface electrodes. Anesth Analg 1968;47(6):717–23.
- [12] Miranda PC, Faria P, Hallett M. What does the ratio of injected current to electrode area tell us about current density in the brain during tDCS? Clin Neurophysiol 2009;120(6):1183–7.
- [13] Deng ZD, Lisanby SH, Peterchev AV. Electric field strength and focality in electroconvulsive therapy and magnetic seizure therapy: a finite element simulation study. J Neural Eng 2011;8(1).
- [14] Wagner T, Fregni F, Fecteau S, Grodzinsky A, Zahn M, Pascual-Leone A. Transcranial direct current stimulation: a computer-based human model study. Neuroimage 2007;35(3):1113–24.
- [15] Bai S, Loo C, Al Abed A, Dokos S. A computational model of direct brain excitation induced by electroconvulsive therapy: comparison among three conventional electrode placements. Brain Stimul 2012;5(3):408–21.
- [16] Song B, Wen P, Ahfock T, Li Y. Numeric investigation of brain tumor influence on the current distributions during transcranial direct current stimulation. IEEE Trans Biomed Eng 2016;63(1):176–87.

- [17] Laakso I, Hirata A. Computational analysis shows why transcranial alternating current stimulation induces retinal phosphores. *J Neural Eng* 2013;10(4).
- [18] Ravnik J, Susnjara A, Tibaut J, Poljak D, Cvetkovic M. Stochastic modelling of nanofluids using the fast boundary-domain integral method. *Eng Anal Bound Elem* 2019;107(2019):185–97.
- [19] Susnjara A, Ravnik J, Verhnyak O, Poljak D, Cvetkovic M. Stochastic-deterministic boundary integral method for transcranial electric stimulation: a cylindrical head representation. In: Proceedings of the 27th international conference on software, telecommunications and computer networks, SoftCOM 2019, Split; 2019.
- [20] Cho JH, Vorwek J, Wolters CH, Knosche TR. Influence of the head model on EEG and MEG source connectivity analyses. *Neuroimage* 2015;110:60–77.
- [21] Cvetkovic M, Dodig H, Poljak D. A study on the use of compound and extracted models in the high frequency electromagnetic exposure assessment. *Math Prob Eng* 2017;12 2017.
- [22] Gabriel C. Compilation of the dielectric properties of body tissues at RF and microwave frequencies. Brooks Air Force Base; 1996. Technical Report: AL/OE-TR-1996-0037, TX:1.
- [23] Gabriel C, Peyman A. Dielectric measurement: error analysis and assessment of uncertainty. *Phys Med Biol* 2006;51(23).
- [24] T and Bahr A, Bolz T, Hennes C. Numerical dosimetry ELF: accuracy of the method, variability of models and parameters, and the implication for quantifying guidelines. *Health Phys* 2007;92(6):521–30.
- [25] Murbach M, Neufeld E, Kainz W, Pruessmann KP, Kuster N. Whole-body and local RF absorption in human models as a function of anatomy and position within 1.5T MR body coil. *Magn Reson Med* 2013;71(2):839–45.
- [26] Poljak D, Cvetkovic M, Bottauscio O, Hirata A, Laakso I, Neufeld E, Reboux S, Warren C, Giannopoulos A, Costen F. On the use of conformal models and methods in dosimetry for nonuniform field exposure. *IEEE Trans Electromagn Compat* 2018;60(2):328–36.
- [27] P.A. Haggall, F. Di Gennaro, C. Baumgartner, E. Neufeld, B. Lloyd, M.C. Gosselin, D. Payne, S. Klingeböck and N. Kuster, "It's database for thermal and electromagnetic parameters of biological tissues," 2018. [Online]. Available: [itis.swiss/database](https://www.itis.swiss.ch/database/). [Accessed 1 September 2019].
- [28] Stenroos M, Mantynen V, Nenonen J. A Matlab library for solving quasi-static volume conduction problems using the boundary element method. *Comput Methods Prog Biomed* 2007;88:256–63.
- [29] Cvetkovic M, Susnjara A, Poljak D, Lallechere S, El Khamlichi Drissi K. Stochastic collocation method applied to transcranial magnetic stimulation analysis. In: Proceedings of the joint annual meeting of the bioelectromagnetics society and the European bioelectromagnetics association, BIOEM 2016. Belgium: Ghent; 2016.
- [30] Cvetkovic M, Poljak D, Haueisen J. Analysis of transcranial magnetic stimulation based on the surface integral equation formulation. *IEEE Trans Biomed Eng* 2015;62(6):1535–45.
- [31] Cvetković M, Poljak D. Electromagnetic-thermal dosimetry comparison of the homogeneous adult and child brain models based on the SIE approach. *J Electromagn Waves Appl* 2015;17:2365–79.
- [32] Weise K, Di Rienzo L, Brauer H, Haueisen J, Toepfer H. Uncertainty analysis in transcranial magnetic stimulation using nonintrusive polynomial chaos expansion. *IEEE Trans Magn* 2015;51(7).
- [33] Codecasa L, Di Rienzo L, Weise K, Gross S, Haueisen J. Fast MOR-based approach to uncertainty quantification in transcranial magnetic stimulation. *IEEE Trans Magn* 2016;52(3):1–4.
- [34] Gomez LJ, Yücel AC, Hernandez-Garcia L, Taylor SF, Michielssen E. Uncertainty quantification in transcranial magnetic stimulation via high-dimensional model representation. *IEEE Trans Biomed Eng* 2015;62(1):361–72.
- [35] Li C, Wu T. Impact of uncertain transcranial magnetic stimulation coil position and orientation in the stimulation for a motor cortex. In: Proceedings of the XXXIInd general assembly and scientific symposium of the international union of radio science, URSI GASS, Montreal, QC, Canada; 2017.
- [36] Schmidt C, Wagner S, Burger M, Rienen U, Carsten HW. Impact of uncertain head tissue conductivity in the optimization of transcranial direct current stimulation for an auditory target. *J Neural Eng* 2015;12(4):1–12.
- [37] Malmivuo J, Plonsey R. Bioelectromagnetism: principles and applications of bioelectric and biomagnetic fields. New York: Oxford University Press; 1995.
- [38] Wrobel LC. The boundary element method. John Wiley & Sons, LTD; 2002.
- [39] Pina HLG, Fernandes JLM, Brebbia DA. Some numerical integration formulae over triangles and squares with a 1/R singularity. *Appl Math Model* 1981;5(3):209–11.
- [40] Papanicolopoulos SA. Efficient computation of cubature rules with application to new asymmetric rules on the triangle. *J Comput Appl Math* 2016;304:73–83.
- [41] Quan W, Evans SJ, Hastings HM. Efficient integration of a realistic two-dimensional cardiac tissue model by domain decomposition. *IEEE Trans Biomed Eng* 1998;45(3):372–85.
- [42] Wandzurat S, Xiao H. Symmetric quadrature rules on a triangle. *Comput Math Appl* 2003;45(12):1829–40.
- [43] Paige CC, Saunders MA. LSQR: an algorithm for sparse linear equations and sparse least squares. *ACM Trans MathSoftw* 1982;8:43–71.
- [44] Loeffler CF, Mansur WJ. Sub-regions without subdomain partition with boundary elements. *Eng Anal Bound Elem* 2016;71:169–73.
- [45] Sobol IM. A primer for the Monte Carlo method. Boca Raton, Florida, USA: CRC Press, Inc; 1994.
- [46] Xiu D. Efficient collocation approach for parametric uncertainty analysis. *Commun Comput Phys* 2007;2(2):293–309.
- [47] Šušnjara A, Dodig H, Cvetković M, Poljak D. Stochastic dosimetry of a three compartment head model. *Eng Anal Bound Elem* 2020;117:332–45.
- [48] Saltelli A, Ratto M, Andres T, Campolongo F, Cariboni F, Gatelli D, Saisana M, Tarantola S. Global sensitivity analysis: the primer. West Sussex, England: John Wiley & Sons, Ltd; 2008.
- [49] Sudret B. Global sensitivity analysis using polynomial chaos expansion. *Reliab Eng Syst Saf* 2008;93(7):964–79.
- [50] Sobol IM. Sensitivity estimates for nonlinear mathematical models. *Mat Model* 1990;2:112–18.